Journal of The Electrochemical Society, **157** (3) H287-H296 (2010)
0013-4651/2010/157(3)/H287/10/$28.00 © The Electrochemical Society

Effects of Surface Forces on Material Removal Rate in Chemical Mechanical Planarization

Dinçer Bozkaya[z] **and Sinan Müftü**[z]

Department of Mechanical Engineering, Northeastern University, Boston, Massachusetts 02115, USA

In chemical mechanical planarization, abrasive particles are pushed onto a wafer by a deformable pad. In addition to the pad–particle contact force, surface forces also act between the wafer and the particles. Experimental studies indicate the significance of slurry pH and particle size on the material removal rate (MRR). In this work, a model for MRR, including the contact mechanics of multiple particles caught in the interface of a rough, porous, and deformable pad and a rigid wafer, including the influences of van der Waals and double-layer forces, is introduced. The effects of surface forces on MRR were investigated for different applied pressures, pad elastic moduli, particle sizes, molar concentrations of ions, and zeta potentials of the wafer and particles. The attractive van der Waals forces increase the MRR, while the double-layer forces, calculated to be repulsive, lower the MRR. The relative magnitude of surface forces compared to the pad–particle force increases with a smaller particle size and a pad elastic modulus. The experimental trends for the variation in MRR with slurry pH were predicted well by the model when the variation in the zeta potential of the wafer and particles with respect to slurry pH is considered.
© 2010 The Electrochemical Society. [DOI: 10.1149/1.3275721] All rights reserved.

Manuscript submitted September 9, 2009; revised manuscript received November 24, 2009. Published January 12, 2010.

Chemical mechanical planarization (CMP) is commonly used in generating planar and smooth surfaces for integrated circuits.[1] In CMP, a rotating wafer is pushed against a rotating polishing pad immersed in a slurry containing chemicals and abrasive particles. High asperities on the wafer surface, passivated by the slurry chemicals, are removed due to the contact with abrasive particles trapped between the pad and the wafer, and as a result, the wafer surface gradually becomes smoother.

Slurry chemicals play an important role for the passivation of the wafer surface. The oxidizers and inhibitors in the slurry determine the reaction kinetics controlling the passivation.[2] The effect of different oxidizers, e.g., hydrogen peroxide (H_2O_2), and inhibitors, e.g., benzotriazole (BTA), on the material removal rate (MRR) was investigated for the CMP of silicon oxide,[3] copper,[4-9] tantalum,[9,10] and tungsten[11,12] films. The reactions with slurry chemicals result in different compositions based on the oxidizer and inhibitor. The overall MRR is influenced by the existence of different compositions on the wafer surface because some of these compositions readily dissolve in the slurry, contributing to the MRR, while some compositions are more difficult to remove from the surface.[5,8] As a result, the surface hardness of the wafer becomes a strong function of the composition, affecting the aggregate wear rate of the wafer material.[4,8,9,11]

In addition to the effect on the wafer hardness, slurry chemicals have also been shown to influence the zeta potential of abrasive particles and the wafer.[3,9,13-15] Experimental studies showed that the citric acid introduced in the slurry causes a significant change in the zeta potential of alumina particles,[16] whereas the zeta potential of silica particles remains almost the same.[15] Luo et al.[14] demonstrated that the addition of BTA reduces the zeta potential of alumina particles. Different ionic salts were also shown to have an influence on the zeta potential.[3] The pH of the slurry was the primary factor affecting the zeta potential of the abrasive particles and the wafer.[17]

The double-layer forces between the wafer and the abrasive particles depend on the zeta potential of both the wafer and the particles. The magnitude of double-layer forces between the wafer and the abrasive particles was shown to have an effect on the MRR.[9,18-21] The MRR is high when the abrasive particles and the wafer are oppositely charged, and a decrease in the MRR is observed as the abrasive particles and the wafer accompany the same charge.[19,20] This behavior was explained by considering the contact force between the wafer and abrasives becoming large when double-layer forces are attractive, causing the MRR for each abrasive to increase.[21] The surface forces also affect the agglomeration of the abrasive particles in the slurry and also the agglomeration of the small wear debris.[22,23] For slurries in which the particles are at their isoelectric point, the particle aggregates can grow from a nanometer to a micrometer size in a relatively short time.[22] Such large particles can be the cause of undesirable, deep scratches on the wafer surface. Chandra et al. reported the depth of the scratches increase with increasing pad hardness and decreasing hardness of the polished layer.[23]

Although the effects of surface forces were shown to have a strong influence on the MRR, as shown in the experiments that were explained earlier, there have been only few models[24-26] developed to understand the experimental trends. The van der Waals forces between the wafer and abrasive particles were considered in a model by Mazaheri and Ahmadi.[24] The inclusion of the van der Waals forces into the model causes an increase in the MRR. In addition, the smaller particle size causes larger MRR due to the influence of the van der Waals forces. This model was improved by including the effect of the roughness of abrasive particles on the magnitude of the van der Waals forces.[24] This was achieved by modeling the abrasive particles as spheres with hemispherical bumps on the surface. Bumpy (rough) abrasive particles were shown to have a lower MRR compared to smooth particles due to the reduction in the van der Waals forces for rough particles. In addition to the van der Waals forces, the electrical double-layer forces were considered in an extension of this model.[25] The experimentally observed variation in the MRR with a slurry pH was attributed to the effect of a slurry pH on the zeta potential, influencing the magnitude of double-layer forces.

The authors introduced a material removal model[27] developed based on the contact interactions between pad, wafer, and abrasive particles.[28] In this model, the contact interactions were modeled at different scales, starting from particle level interactions and gradually expanding the contact scale to the multiasperity contact between the pad and the wafer (Fig. 1). The applied pressure, distributed to a three-body contact due to the abrasive particles caught between the pad and the wafer and a two-body contact between the pad and the wafer, was calculated by the model. The model was used to explain the effects of important parameters such as the elastic modulus of the solid pad material E_s, equivalent elastic modulus for the porous pad E_p, standard deviation (STD) of the abrasive particle size σ_p, probability density function (PDF) of the abrasive size distribution Φ_p, particle weight concentration η_w, STD of pad asperity peak heights σ_s, average radius of pad asperities R_s, PDF of pad asperity heights Φ_s, wafer hardness H_w, and applied pressure P_o. The objective of this work is to extend this model to include the effects of surface forces. In addition to the force applied on the abrasive by the pad, the contribution of the surface forces acting between the wafer and the abrasive particles to the overall force equilibrium at the

[z] E-mail: bozkaya@coe.neu.edu; s.muftu@neu.edu

Downloaded 12 Jan 2010 to 129.10.64.116. Redistribution subject to ECS license or copyright; see http://www.ecsdl.org/terms_use.jsp

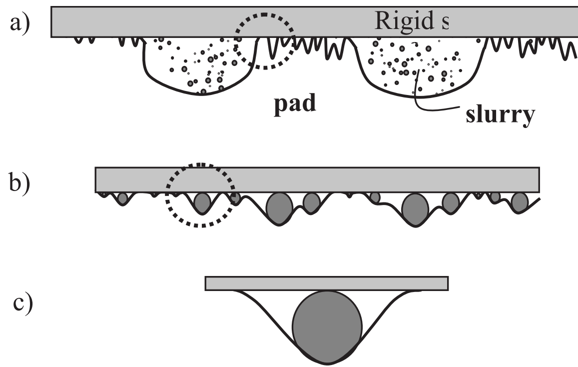

Figure 1. Different scales of contact: (a) Multiasperity contact, (b) multi particle contact, and (c) single particle contact.

wafer–abrasive interface is considered (Fig. 2). As a result of this improvement, the model enables the calculation of the MRR by including the effects of the effective Hamaker constant A_{wsp} between the wafer and the particles and the zeta potential $\Psi_{1,2}$ of the wafer and particles in the following form

$$RR = k_w(E_s, E_s/E_p, \sigma_p, \eta_w, \sigma_s, R_s, A_{wsp}, \Psi_{1,2}, H_w) f(P_o) V_r \quad [1]$$

where the function f describes the variation in the MRR with P_o, and V_r is the relative sliding velocity between the wafer and the pad. Note that the presence of the slurry in the wafer–pad interface causes elastohydrodynamic lubrication conditions both at the pad–wafer[29] and asperity–wafer interaction scales.[30] These effects are not considered in this work.

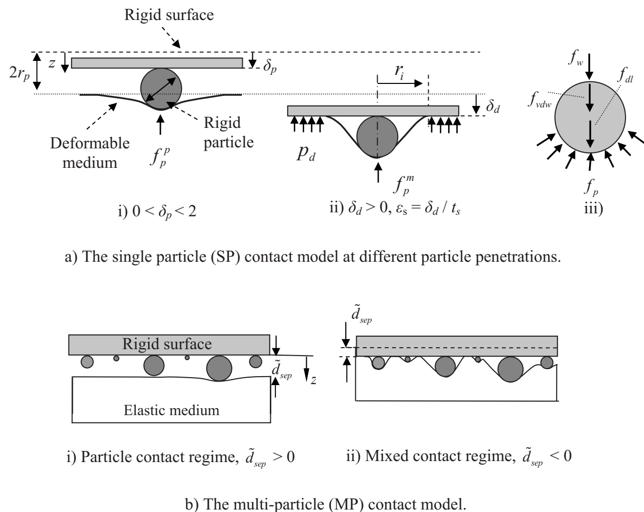

Figure 2. Details and definitions used in the SP and MP models.

Pad–Particle Contact

The contact of a single abrasive particle is modeled in a single particle (SP) contact model, where the three-body contact of one spherical rigid particle, one deformable, and one rigid flat surface is analyzed by using the finite element method.[28] In the particle contact regime, the penetration of the particle δ_p in the pad is less than a diameter of the particle [Fig. 2a(i)] $0 < \delta_p < 2r_p$, and the particle contact force f_p^p can be obtained by the curve-fitting of modeling results as follows[28]

$$f_p^p = \frac{E_s}{1-\nu_s^2} r_p^2 \left[\frac{4}{3}\left(\frac{\delta_p}{r_p}\right)^{3/2} - 0.10\left(\frac{\delta_p}{r_p}\right)^{2.89} \right] \quad \text{for } 0 < \delta_p < 2r_p \quad [2]$$

In the mixed contact regime $\delta_p > 2r_p$, the pad–wafer direct contact occurs in addition to the particle contact [Fig. 2a(ii)]. The particle contact force f_p^m in this regime can be expressed as follows[28]

$$f_p^m = \frac{E_s}{1-\nu_s^2} r_p^2 \begin{cases} 5.4(\varepsilon_s)^{0.57} + 3.12, & \text{for } 0 < \varepsilon_s < 0.05 \\ 11.1(\varepsilon_s - 0.05)^{0.90} + 4.10, & \text{for } 0.05 < \varepsilon_s < 0.2 \\ 40.94(\varepsilon_s - 0.2)^2 + 13.14(\varepsilon_s - 0.2) + 6.11, & \text{for } 0.2 < \varepsilon_s < 0.45 \end{cases} \quad [3]$$

where ε_s is the average compressive strain $\varepsilon_s = \delta_d/t_s$, defined as the ratio of the pad displacement δ_d due to the direct contact to the pad thickness t_s. The direct contact pressure p_d^m at the pad–wafer interface can be calculated by using the following relationship[28]

$$p_d^m = \frac{E_s}{1-\nu_s^2} \begin{cases} 0.76\varepsilon_s, & \text{for } 0 < \varepsilon_s < 0.015 \\ 0.85(\varepsilon_s - 0.015) + 0.011, & \text{for } 0.015 < \varepsilon_s < 0.2 \\ 1.8(\varepsilon_s - 0.2)^{1.16} + 0.17, & \text{for } 0.2 < \varepsilon_s < 0.45 \end{cases} \quad [4]$$

The influence radius r_i is the radius of the circular noncontact area around each particle [Fig. 2a(ii)]. The influence radius r_i can be found as follows[28]

$$r_i = 1.52 r_p (\varepsilon_s)^{-0.45} \quad \text{for } 0 < \varepsilon_s < 0.45 \quad [5]$$

Once the relationships for each particle are determined by the SP contact model, the contact of active particles at the pad–wafer interface is modeled in the multiparticle (MP) contact model. In the particle contact regime [Fig. 2b(i)], the number of active particles η_a^{mp} in contact can be determined for a given local separation distance d_{sep} by using the slurry volume between the pad and the wafer as

$$\eta_a^{mp}(d_{sep}) = \eta_v \int_{d_{sep}/2}^{\infty} 2r_p \Phi_p(r_p) dr_p \quad [6]$$

where Φ_p is the probability distribution function for the particle radii and η_v is the number of particles per unit slurry volume. The particle concentration by weight ratio η_w is a common measure for the particle concentration and can be converted into a volumetric particle concentration η_v by using the following relationship[28]

Downloaded 12 Jan 2010 to 129.10.64.116. Redistribution subject to ECS license or copyright; see http://www.ecsdl.org/terms_use.jsp

$$\eta_v = \frac{\rho_s}{\rho_p} \frac{\eta_w}{\int_0^\infty \frac{4}{3}\pi r_p^3 \Phi_p(r_p) dr_p} \quad [7]$$

where ρ_p and ρ_s are the mass densities of the particles and slurry, respectively.

In the particle contact regime $d_{sep} > 0$ [Fig. 2b(i)], all the load is carried by particle contacts, which is determined by integrating the force on each particle given by the load-displacement function f_p^p from Eq. 2 over all active particles η_a^{mp} in contact (Eq. 6) as follows[28]

$$p_p^{mp\text{-}p} = \frac{E_s}{1-\nu_s^2}\eta_v \int_{d_{sep}/2}^{\infty} 2r_p f_p^p(\delta_p)\Phi_p(r_p) dr_p \quad \text{for } d_{sep} > 0 \quad [8]$$

where the penetration of each particle δ_p is defined as $\delta_p = (2r_p - d_{sep})$.

In the mixed contact regime $d_{sep} < 0$ [Fig. 2b(ii)], the mean contact pressure p_c^{mp} consists of a contact pressure due to the particle and direct contact as $p_c^{mp} = p_p^{mp\text{-}m} + p_d^{mp}$. The mean contact pressure $p_p^{mp\text{-}m}$ due to particle contacts is found by using the following relationship[28]

$$p_p^{mp\text{-}m} = \frac{E_s}{1-\nu_s^2}\eta_v \int_0^{\infty} 2r_p f_p^m(-\varepsilon_p)\Phi_p(r_p) dr_p \quad \text{for } d_{sep} < 0 \quad [9]$$

Note that the number of active particles η_a^{mp} from Eq. 6 remains constant in this regime. The mean direct contact pressure p_d^{mp} is calculated by considering the direct contact area A_d^{mp} developing between the pad and the wafer and the direct contact pressure function p_d^m given by Eq. 4 as[28]

$$p_d^{mp} = \frac{E_s}{1-\nu_s^2}\int_{\varepsilon_p^m}^{\varepsilon_p} p_d^m(\varepsilon_p^r - \varepsilon_p)\frac{dA_d^{mp}}{d\varepsilon_p^r} d\varepsilon_p^r \quad [10]$$

The direct contact area is determined by subtracting the influence contact area of active particles from the total contact area, $A_d^{mp} = 1 - A_i$. The total influence area of particles as a fraction of the total area A_i can be found by the summation of the influence areas of individual particles πr_i^2 as follows[28]

$$A_i^{mp} = \eta_v \int_0^{\infty} 2r_p \pi r_i^2(-\varepsilon_p)\Phi_p(r_p) dr_p \quad [11]$$

where r_i is given by Eq. 5.

Wafer–Particle Contact

The wafer–particle contact force f_w consists of the force transmitted through the pad–particle contact f_p and surface forces f_s between the wafer and the particle, including the van der Waals f_{vdW} and electrical double-layer forces f_{dl} as follows

$$f_w = f_p + f_s = f_p + f_{vdW} + f_{dl} \quad [12]$$

The free body diagram of a particle under the effect of this force is shown in Fig. 2a(iii). The van der Waals force for the contact of one rigid spherical particle with radius r_p and one rigid flat surface can be found by using[31]

$$f_{vdW} = \frac{A_{wsp}}{6d_o^2} r_p \quad [13]$$

where d_o is the equilibrium separation distance and A_{wsp} is the effective Hamaker constant. The effective Hamaker constant A_{wsp} between the wafer and the particle in a slurry can be determined by using the Hamaker constant of the wafer A_w, the particle A_p, and the slurry A_s as follows[32]

$$A_{wsp} = (A_w^{1/2} - A_s^{1/2})(A_p^{1/2} - A_s^{1/2}) \quad [14]$$

When an uncharged particle is placed in a liquid, the particle acquires a surface charge, which creates an electrostatic field and affects the ions in the bulk liquid. The electric field around the charged particle attracts the ions of the opposite sign (counter-ions) and repels the ions of the same sign (co-ions).[33] As a result, two layers of positive and negative ions form around each particle named as the double layer. As two charged particles approach each other, the double layers of the particles start to overlap,[33] causing interaction forces between the particles. The interaction forces become significant when the distance between the particles becomes less than the Debye length $1/\kappa$, which is the reciprocal of κ expressed as follows[33]

$$\kappa^2 = (e^2/\varepsilon\varepsilon_o kT)\sum_i z_i^2 n_{i\infty} \quad [15]$$

where e is the electrical charge, ε is the dielectric constant of medium, ε_o is the dielectric permittivity of vacuum, z_i is the valence number, k is the Boltzmann constant, T is the temperature, and $n_{i\infty}$ is the concentration of ions far away from the surface. Note that the subscript i indicates the possibility of different ionic species in the solution. The concentration of ions $n_{i\infty}$ can be calculated by using the molar concentration of the electrolyte M_i as follows[33]

$$n_{i\infty} = 1000 N_A M_i \quad [16]$$

where N_A is Avogadro's number (6.02×10^{23}) and M_i (mol/liter) is the molar concentration of the electrolyte in the liquid.

Different assumptions are used to derive the double-layer force between two charged particles. The Hogg–Healy–Fuerstenau (HHF) equations for the constant charge (CC)[34,35] assumption and the compression approximation (CA) used by Gregory[36] are employed in this work to calculate the double-layer forces between the wafer and the particle. These approaches were shown to be accurate especially when the separation distance between the surfaces is small,[33,37] which is the case for the contacting wafer and particles.

The double-layer interaction force f_{dl} between one spherical particle with radius r_p and flat surface and zeta potentials Ψ_1 and Ψ_2 under a constant surface charge assumption (HHF-CC)[34,35] is given as a function of the separation distance d_o as follows

$$f_{dl}(d_o) = -2r_p\pi\varepsilon_o\varepsilon_r(\Psi_1^2 + \Psi_2^2)\frac{\kappa e^{-\kappa d_o}}{1 - e^{-2\kappa d_o}}\left(\frac{2\Psi_1\Psi_2}{\Psi_1^2 + \Psi_2^2} + e^{-\kappa d_o}\right) \quad [17]$$

The double-layer force between two spherical particles can be computed based on the CA [36] as follows

$$f_{dl}(d_o) = \frac{-4r_p\pi n_\infty kT}{\kappa}\left[2\bar{y}\ \ln\left(\frac{B + \bar{y}\ \coth(\kappa d_o/2)}{1 + \bar{y}}\right) - \ln(\bar{y}^{-2} + \cosh\ \kappa d_o + B\ \sinh\ \kappa d_o) + \kappa d_o\right] \quad [18]$$

where $n_\infty = \Sigma_i n_{i\infty}$, $\bar{y} = y_1 + y_2$, $y = ze\Psi/kT$, and $B = [1 + \bar{y}^2\ \csc\ h^2(\kappa d_o/2)]^{1/2}$.

MRR

The calculation of the removal force function (RFF) for an SP is explained first, and then the integration of the RFF of an SP over all active particles captured in the contact area between the pad and the wafer is described.

RFF due to pad–wafer local contact.— Next, the wear rate relationships are introduced for a rigid spherical particle sliding with velocity V_r over a wafer with hardness H_w under the influence of a normal force f_w. Both adhesive and abrasive wear mechanisms are considered. In the adhesive wear, the wear rate RR_{ad}^{sp} is linearly proportional to the wafer–particle contact force f_w as follows[38]

$$RR_{ad}^{sp} = \frac{k_w^{ad} V_r}{H_w} f_w \quad [19]$$

where k_w^{ad} is an empirically determined adhesive wear coefficient.

Downloaded 12 Jan 2010 to 129.10.64.116. Redistribution subject to ECS license or copyright; see http://www.ecsdl.org/terms_use.jsp

The abrasive wear rate RR_{ab}^{sp} for an SP can be found by considering the sliding indentation of a particle in a wafer with a perfectly plastic deformation[27] as

$$RR_{ab}^{sp} = \left(\frac{k_w^{ab} V_r}{H_w^{3/2}}\right)\sqrt{\frac{2}{\pi^3}}\frac{f_w^{3/2}}{r_p} \quad [20]$$

The MRR is investigated in our models by calculating the RFF for the adhesive R_{ad}^{sp} and abrasive R_{ab}^{sp} wear, which is a measure of mechanical action causing a material removal. The RFF is defined as follows

$$R_{ad}^{sp} = f_w \quad [21]$$

$$R_{ab}^{sp} = \sqrt{\frac{2}{\pi^3}}\frac{f_w^{3/2}}{r_p} \quad [22]$$

for adhesive and abrasive wear cases based on Eq. 19 and 20. Once the RFF of an SP R^{sp} is determined using Eq. 21 and 22, the RFF, due to multiple particles trapped between two flat surfaces, can be found in a way similar to Eq. 8 and 9 for a particle contact pressure p_p^{mp} in the MP contact model. This gives the following relationship for the RFF for multiple particles

$$R^{mp} = \begin{cases} \eta_v \int_{d_{sep}/2}^{\infty} 2r_p R^{sp}\Phi_p(r_p)dr_p & \text{if } d_{sep} > 0 \\ \eta_v \int_{0}^{\infty} 2r_p R^{sp}\Phi_p(r_p)dr_p & \text{if } d_{sep} < 0 \end{cases} \quad [23]$$

Note that R^{mp} given in Eq. 23 is a function of the separation distance d_{sep}. However, from a practical point of view, it makes more sense to report the RFF as a function of the contact pressure p_c^{mp} acting between the two surfaces. To obtain the RFF as a function of the contact pressure p_c^{mp}, the separation distance d_{sep} is used as an intermediate parameter, and the RFF is matched against the contact pressure p_c^{mp} by using look-up tables created for relating both p_c^{mp} and the RFF to d_{sep} using Eq. 8-10 and 23. In fact, a similar approach is used to estimate other parameters such as the particle contact pressure ratio p_p^{mp}/p_c^{mp} and the direct contact area ratio A_d^{mp} as a function of the contact pressure p_c^{mp}.

RFF due to pad–wafer rough contact.— In the MP contact model, the local pad–wafer contact is characterized. However, the pad–wafer contact occurs at the tip of the pad asperities with different heights due to the pad roughness. Therefore, the local contact pressure at each asperity tip is different. To capture this effect, the real mean contact pressure at each asperity tip is introduced in the MP contact model, and the outputs of the MP contact model are integrated over all contacting asperities. The real mean contact pressure and the contact area at an asperity can be found using the Hertzian relationships[39] as

$$p_c^m = \frac{4E_p}{3\pi(1-\nu_p^2)}\left(\frac{\delta_s}{R_s}\right)^{1/2} \quad \text{and} \quad a = (\delta_s R_s)^{1/2} \quad [24]$$

where E_p is the elastic modulus of the porous pad and δ_s is the pad asperity deformation. The deformation of each asperity is determined by the peak height of asperities z_s and equilibrium separation distance d_{wp} between the pad and the wafer as $\delta_s = z_s - d_{wp}$. The applied pressure P_o and equilibrium separation distance d_{wp} are related as[39]

$$P_o = \frac{4}{3}\eta_s E_p R_s^{1/2}\int_{d_{wp}}^{\infty}\Phi_s(z_s)(z_s - d_{wp})^{3/2}dz_s \quad [25]$$

where η_s is the areal density of the pad asperity peaks, R_s is the asperity radius, and Φ_s is the PDF of asperity peaks heights. The RFF between the pad and the wafer is found by using the following relationship

Table I. Physical values of parameters.

Parameter	Base
Particle concentration (η_w)	2.5%
Particle to slurry density ratio (ρ_p/ρ_s)	3.7 (alumina)
Pad summit radius (R_s)	50 μm
Pad summit density (η_s)	$2 \times 10^{-4}/\mu m^2$
Pad summit STD (σ_s)	5 μm
Applied pressure (P_o)	0.007 MPa (1 psi)

$$R = \eta_s \int_{d_{wp}}^{\infty} \pi a^2 R^{mp}(p_c^m)\Phi_s(z_s)dz_s \quad [26]$$

Results

The parameters used in the calculations are listed in Table I. The contacting surfaces are assumed to be atomically smooth, i.e., equilibrium separation distance $d_o = 4$ Å. The effects of the van der Waals and double-layer forces on the RFF are studied next.

Effect of van der Waals force on RFF.— The van der Waals forces f_{vdW} between the wafer and the particles is calculated using Eq. 13. The van der Waals forces f_{vdW} are always attractive, and their magnitude depends on the separation distance d_o, particle size μ_p, and effective Hamaker constant A_{wsp}. The effective Hamaker constant A_{wsp} is calculated considering the effect of the medium (slurry) between the wafer and the particle using Eq. 14. Due to the low Hamaker constant of the slurry (water), $A_s = 4.38 \times 10^{-20}$ J,[32] the effective Hamaker constant in the slurry is smaller than that in nitrogen (N_2), as illustrated by the measurements[40] listed in Table II. Considering the variation in the effective Hamaker constant A_{wsp} between alumina (Al_2O_3) and various wafer materials in water, 1.3×10^{-20} J $< A_{wsp} < 6.6 \times 10^{-20}$ J,[40] A_{wsp} was varied in the range of 1×10^{-20} J $< A_{wsp} < 5 \times 10^{-20}$ J in the simulations.

Figure 3 illustrates the variation in RFF due to the adhesive (Fig. 3a) and the abrasive wear (Fig. 3b) in the presence of the van der Waals force for a soft pad $E_s = 10$ MPa with a porous elastic modulus ratio $E_s/E_p = 4$ and a mean particle radius of $\mu_p = 5$ nm. The van der Waals force f_{vdW} enhances the RFF due to both the adhesive R_{ad} and the abrasive wear R_{ab}, and the effect becomes more significant with the higher effective Hamaker constant A_{wsp}. Figure 3 demonstrates that the increase in the RFF due to the abrasive wear R_{ab} is larger than that of the RFF due to the adhesive wear R_{ad}.

The effect of the van der Waals force f_{vdW} on the RFF can be quantified by the ratio of the change in RFF due to the presence of the van der Waals force ΔR^s to the RFF in the absence of the van der Waals force R as $\Delta R^s/R$. This parameter is plotted in Fig. 4 as a function of the solid-pad elastic modulus E_s, with $E_s/E_p = 4$ and $A_{wsp} = 5 \times 10^{-20}$ J for both the adhesive and abrasive wear assumptions. This figure shows that the relative effect of the van der Waals force $\Delta R/R$ increases as the pad elastic modulus E_s and particle size μ_p become smaller. The increase in the RFF due to the presence of the van der Waals force $\Delta R^s/R$ may be as large as 44%

Table II. Hamaker constant of alumina (Al_2O_3) with different materials in water and nitrogen.[40]

System	A_{wsp} ($\times 10^{-20}$ J)
$Cu/N_2/Al_2O_3$	21.7
$SiO_2/N_2/Al_2O_3$	9.7
$W/N_2/Al_2O_3$	22.6
$Cu/H_2O/Al_2O_3$	6.2
$SiO_2/H_2O/Al_2O_3$	1.3
$W/H_2O/Al_2O_3$	6.6

Downloaded 12 Jan 2010 to 129.10.64.116. Redistribution subject to ECS license or copyright; see http://www.ecsdl.org/terms_use.jsp

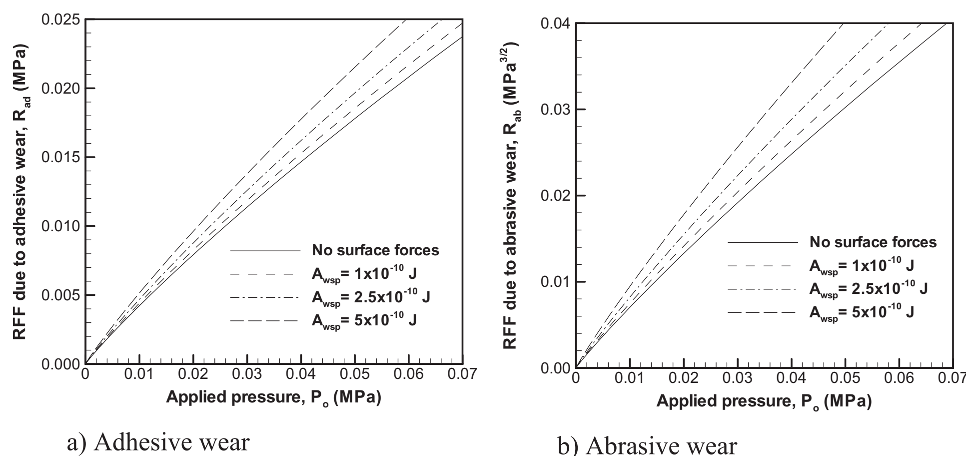

a) Adhesive wear b) Abrasive wear

Figure 3. The effect of van der Waals force on the RFF due to (a) adhesive wear R_{ad} and (b) abrasive wear R_{ab} for a soft $E_s = 10$ MPa, porous pad $E_s/E_p = 4$, and mean particle radius $\mu_p = 5$ nm.

for the adhesive wear and 73% for the abrasive wear for the equivalent Hamaker constant $A_{wsp} = 5 \times 10^{-20}$ J, pad elastic modulus $E_s = 10$ MPa, and mean particle radius $\mu_p = 2.5$ nm. The effect of the van der Waals force f_{vdW} on the RFF due to the adhesive wear R_{ad} becomes less than 5% $\Delta R^s/R < 0.05$ when the pad elastic modulus is greater than $E_s > 80$ MPa ($\mu_p = 2.5$ nm) or the particle radius is larger than $\mu_p > 30$ nm ($E_s = 10$ MPa).

Effect of double-layer forces on RFF.— Equations 17 and 18 are used to calculate the double-layer force f_{dl} acting between the wafer and the particles. These equations were developed based on two different assumptions, the Hogg–Healy–Fuerstenau constant charge (HHF-CC) and the CA. The parameters used in the calculations of the double-layer force are listed in Table III. Figures 5 and 6 show the RFF in the presence of the double-layer force f_{dl} calculated by the CA and HHF-CC assumptions, respectively. In addition to the base parameters listed in Table I, the pad elastic modulus and the mean particle radius are taken to be $E_s = 10$ MPa with $E_s/E_p = 4$ and $\mu_p = 5$ nm, respectively.

The presence of double-layer forces f_{dl} causes the RFF to decrease when CA is used to calculate f_{dl} even when the wafer and particle are oppositely charged ($\Psi_{1,2} = 50$ mV, -25 mV), as shown in Fig. 5. According to the CA assumption, the magnitude of double-layer forces becomes zero $f_{dl} = 0$ when the wafer and particle are oppositely charged with the same zeta potential, e.g., $\Psi_{1,2} = 50$ mV, -50 mV. As the sum of zeta potentials $(\Psi_1 + \Psi_2)$ increases, the effect of double-layer forces f_{dl} becomes more important. It is seen in Fig. 6 that the magnitude of double-layer forces f_{dl} calculated by the HHF-CC assumption is larger than that of the CA assumption; therefore, there is a greater effect of f_{dl} on the RFF when the HHF-CC assumption is employed. In contrast to the CA assumption, the HHF-CC assumption predicts a slightly attractive double-layer force increasing the RFF when the surface is oppositely charged with high zeta potentials, e.g., $\Psi_{1,2} = 50$ mV, -50 mV. The effect of double-layer forces f_{dl} on the RFF is greater in the abrasive wear (Fig. 5b and 6b) compared to that in the adhesive wear (Fig. 5a and 6a).

The relative effect of double-layer forces f_{dl} on the RFF for different particle radii μ_p and pad elastic moduli E_s is further evaluated in Fig. 7 (CA) and Fig. 6 (HHF-CC), where the zeta potentials of the wafer and the particle are taken to be $\Psi_{1,2} = 50$ and 50 mV, respectively, the molar concentration $M = 0.01$, and the porous elastic modulus ratio $E_s/E_p = 4$. Note that the change in RFF due to the presence of double-layer forces $\Delta R^s/R$ is negative because double-layer forces f_{dl} are repulsive under these conditions. According to the predictions for the double-layer force f_{dl} using the CA assumption shown in Fig. 7, the effect of the double-layer force is less than 10%, $\Delta R^s/R < 0.10$ in the range of particle sizes of 2.5 nm $< \mu_p < 40$ nm, and the pad elastic modulus 10 MPa $< E_s < 100$ MPa studied. The calculations using the HHF-CC assumption (Fig. 8) yields a much higher magnitude for the double-layer force f_{dl}, and the effect is predicted to be as large as $\Delta R^s/R = 0.60$ when a small particle radius $\mu_p = 2.5$ nm and a soft pad $E_s = 10$ MPa are used.

In Fig. 9, the effect of the molar concentration M on the RFF due to the adhesive wear R_{ad} is investigated for the different equilibrium separation distance d_o values for CA (Fig. 9a) and HHF-CC (Fig. 9b) approximations. Note that the effect seen in the abrasive wear is similar. The calculations are performed for a soft pad E_s

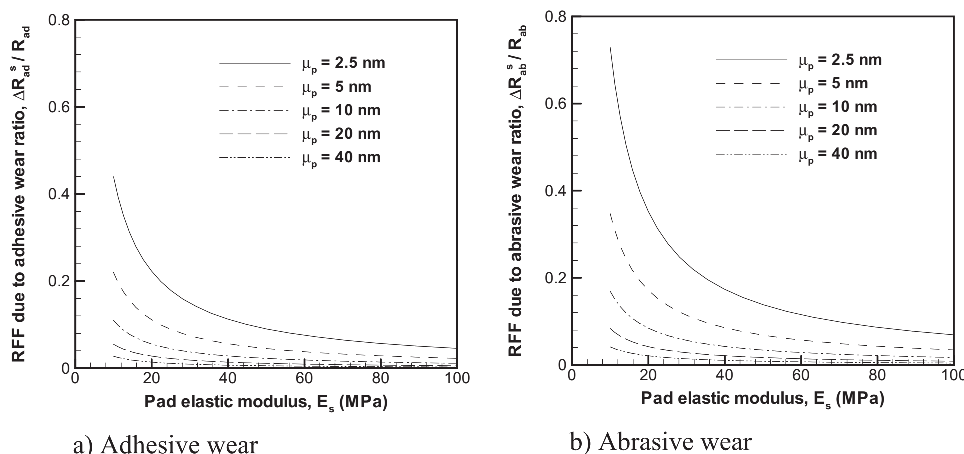

a) Adhesive wear b) Abrasive wear

Figure 4. The effect of van der Waals force on (a) RFF due to adhesive wear R_{ad} and (b) RFF due to abrasive wear R_{ab} quantified by the ratio of change in R due to surface forces, ΔR^s and $\Delta R^s/R$, for different pad elastic modulus E_s ($E_s/E_p = 4$) and mean particle radius μ_p ($A_{wsp} = 5 \times 10^{-20}$ J).

Downloaded 12 Jan 2010 to 129.10.64.116. Redistribution subject to ECS license or copyright; see http://www.ecsdl.org/terms_use.jsp

Table III. Parameters used for the calculation of double-layer forces.

Parameter	Value
Electron charge (e)	1.6×10^{-19} C
Avagadro's number (N_a)	6.02×10^{23}
Dielectric constant of water (ε_r)	78.4
Permittivity of vacuum (ε_o)	8.85×10^{-12} C^2 N^{-1} m^{-2}
Temperature (T)	298 K
Boltzmannn constant (k)	1.38×10^{-23}
Valence (z)	1

= 10 MPa with a porous elastic modulus ratio $E_s/E_p = 4$, a particle size $\mu_p = 5$ nm, a zeta potential $\Psi_{1,2} = 50$ mV, 50 mV, and an applied pressure $P_o = 0.007$ MPa. An opposite trend is observed for the magnitude of the double-layer force f_{dl} calculated by the CA and HHF-CC assumptions where a larger molar concentration M causes the magnitude f_{dl} to increase for the CA assumption, while f_{dl} for the HHF-CC assumption decreases with larger M. Larger separation distance d_o has a negative effect on the magnitude of double-layer forces for both the CA and HHF-CC assumptions.

The RFF R given in Eq. 27 depends on the mean particle size μ_p as the surface force for an SP depend on its size r_p (Eq. 13 and 18). If the surface forces f_s are attractive, then smaller particles (i.e., smaller μ_p) result in a larger RFF, and the effect of f_s on the RFF depends on the relative magnitude of the pad-particle contact force

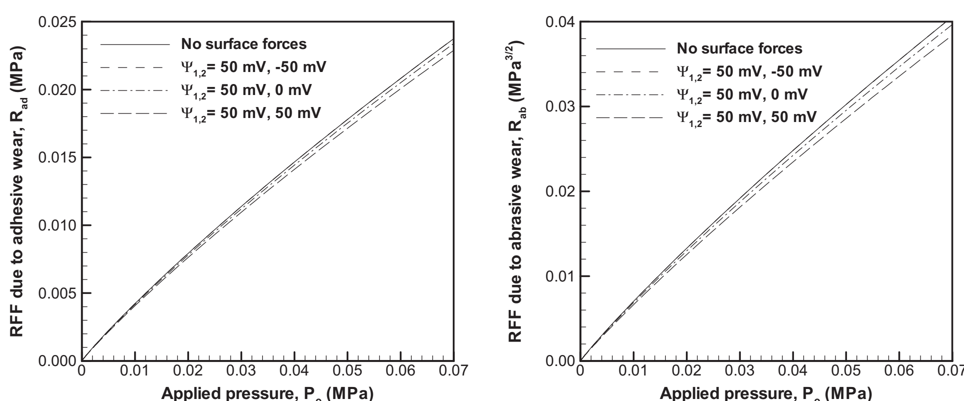

Figure 5. The effect of double-layer force calculated by CA assumption on RFF due to (a) adhesive wear R_{ad} and (b) abrasive wear R_{ab} for a soft $E_s = 10$ MPa, porous pad $E_s/E_p = 4$, and mean particle radius $\mu_p = 5$ nm.

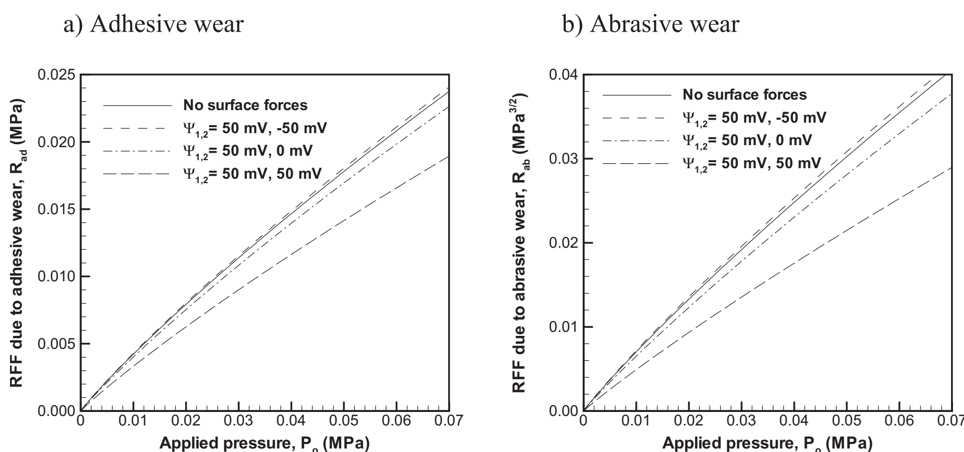

Figure 6. The effect of double-layer force calculated by HHF-CC assumption on RFF due to (a) adhesive wear R_{ad} and (b) abrasive wear R_{ab} for a soft $E_s = 10$ MPa, porous pad $E_s/E_p = 4$, and mean particle radius $\mu_p = 5$ nm.

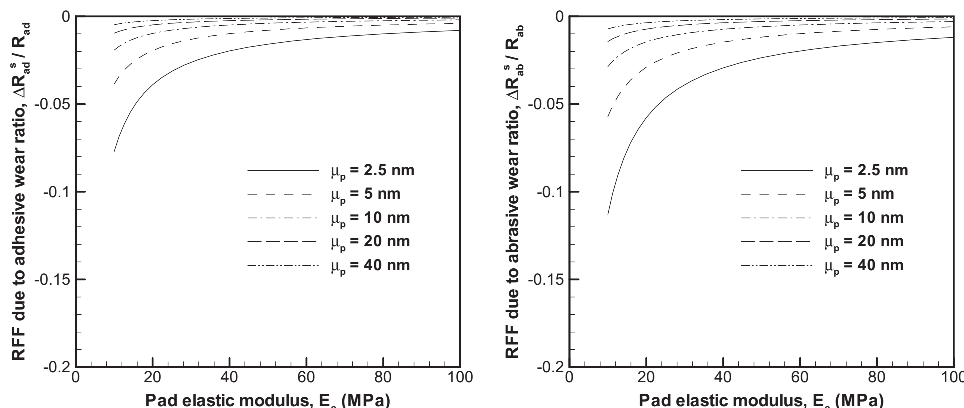

Figure 7. The effect of double-layer force on (a) RFF due to adhesive wear R_{ad} and (b) RFF due to abrasive wear R_{ab} quantified by the ratio of change in R due to surface forces, ΔR^s and $\Delta R^s/R$, for different pad elastic modulus E_s ($E_s/E_p = 4$) and mean particle radius μ_p ($\Psi_{1,2}$ = 50 mV, 50 mV, and $M = 0.01$). CA assumption is used to calculate double-layer force.

Downloaded 12 Jan 2010 to 129.10.64.116. Redistribution subject to ECS license or copyright; see http://www.ecsdl.org/terms_use.jsp

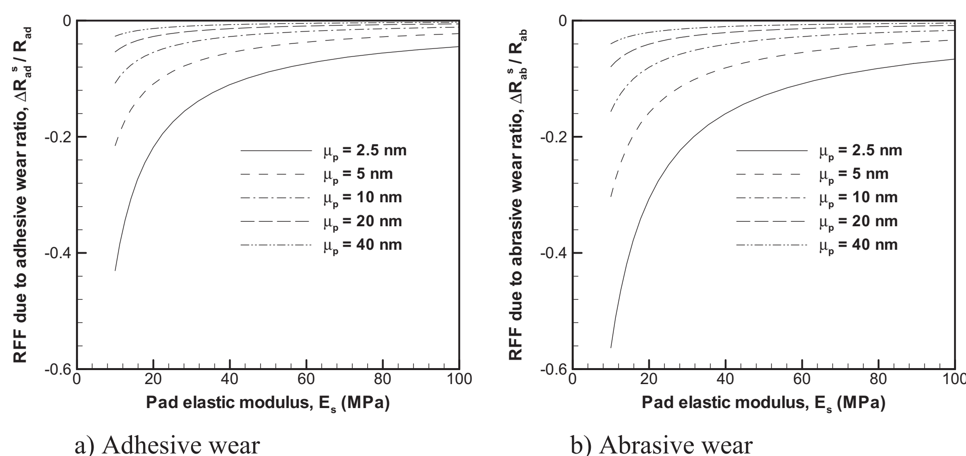

Figure 8. The effect of double-layer force on (a) RFF due to adhesive wear R_{ad} and (b) RFF due to abrasive wear R_{ab} quantified by the ratio of change in R due to surface forces, ΔR^s and $\Delta R^s/R$, for different pad elastic modulus E_s ($E_s/E_p = 4$) and mean particle radius μ_p ($\Psi_{1,2}$ = 50 mV, 50 mV, and M = 0.01). HHF-CC assumption is used to calculate double-layer force.

f_p. If surface forces f_s are repulsive, then f_s has a negative effect on the RFF, causing the RFF to decrease with a smaller particle size μ_p. This is illustrated in Fig. 10, where the variation in RFF is plotted as a function of the mean particle radius μ_p in the presence of the attractive van der Waals f_{vdW} and repulsive double-layer forces f_{dl}. The calculations are performed for a soft pad $E_s = 10$ MPa with a porous elastic modulus ratio $E_s/E_p = 4$. Double-layer forces f_{dl} are calculated using the HHF-CC assumption. Figure 10 shows that the magnitude of surface forces f_s becomes small compared to the pad–particle contact force f_p for the particle radius $\mu_p > 20$ nm; therefore, the RFF remains constant with respect to μ_p. Note that the effect of the particle size μ_p due to the influence of surface forces f_s becomes more important as the magnitude of f_s increases.

Comparison with experimental results.— CMP experiments were carried out by Ramarajan et al. to investigate the effect of slurry pH on the MRR of tantalum films polished by slurries containing silica and alumina particles.[19] The zeta potentials of tantalum pentoxide, alumina, and silica were determined as a function of pH and were described by the following curve-fit equations[25]

$$\Psi_{\text{tantalum}} = \begin{cases} 80 \text{ mV} & \text{pH} \le 2 \\ 80 \cos\dfrac{\pi(\text{pH}-1.8)}{10} \text{ mV} & 2 \le \text{pH} \le 12 \\ -80 \text{ mV} & \text{pH} \ge 12 \end{cases} \qquad [27a]$$

$$\Psi_{\text{alumina}} = \begin{cases} 25 \text{ mV} & \text{pH} \le 7.4 \\ 25 \cos\dfrac{\pi(\text{pH}-7.4)}{4.6} \text{ mV} & 7.4 \le \text{pH} \le 12 \\ -25 \text{ mV} & \text{pH} \ge 12 \end{cases} \qquad [27b]$$

$$\Psi_{\text{silica}} = \begin{cases} 25 \cos\dfrac{\pi(\text{pH})}{4.2} \text{ mV} & \text{pH} \le 4.2 \\ -25 \text{ mV} & \text{pH} \ge 4.2 \end{cases} \qquad [27c]$$

Equation 27 shows that the zeta potential is positive for all materials at small pH. As pH increases, the zeta potential Ψ decreases and Ψ becomes negative $\Psi < 0$ for pH above the isoelectric point. This point is located at pH 6.8 for tantalum pentoxide, pH 9.7 for alumina, and pH 2.1 for silica. Based on these results, it is determined that the tantalum pentoxide wafer and the alumina particle are oppositely charged when pH is in the range of $6.8 < \text{pH} < 9.7$. The same condition appears for the tantalum pentoxide wafer and the silica particle for $2.1 < \text{pH} < 6.8$.

The variation in the MRR, normalized with respect to the maximum MRR, in tantalum CMP experiments[19] with alumina and silica slurries is plotted as a function of slurry pH in Fig. 11. Experimental results show that the MRR is a strong function of the slurry pH. This was attributed to the effect of double-layer forces f_{dl} varying in magnitude with slurry pH. The model developed in this work was implemented by using the parameters of the experimental condi-

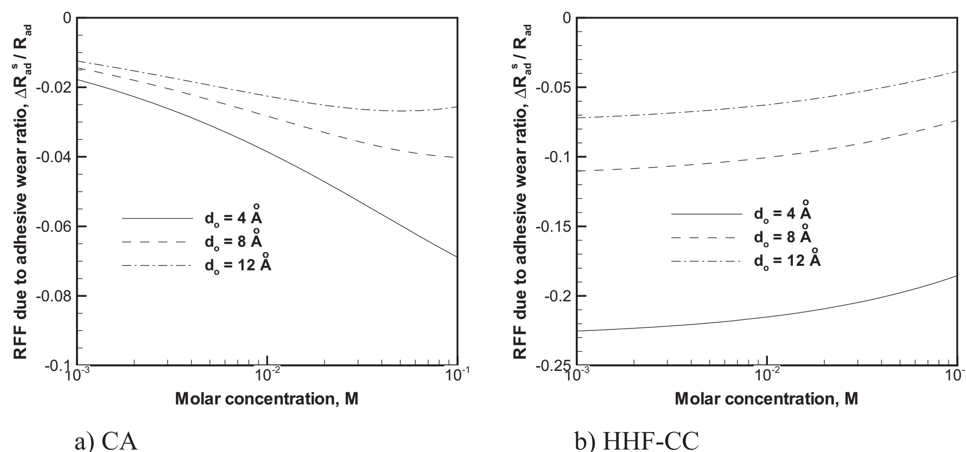

Figure 9. The effect of double-layer force on RFF due to adhesive wear R_{ad} quantified by $\Delta R^s/R$ for different separation distance d_o and molar concentration calculated by (a) CA and (b) HHF-CC assumptions. ($\Psi_{1,2}$ = 50 mV, 50 mV, μ_p = 5 nm, E_s = 10 MPa, E_s/E_p = 4, and P_o = 0.007 MPa).

Downloaded 12 Jan 2010 to 129.10.64.116. Redistribution subject to ECS license or copyright; see http://www.ecsdl.org/terms_use.jsp

tions. In the model, the slurry pH influences the zeta potential of the wafer and the particle, as described by Eq. 27; therefore, the contact force between the wafer and the particle f_w varies with slurry pH. The elastic modulus of a soft pad ($E_s = 1$ MPa and $E_s/E_s = 4$) and a particle concentration of $\eta_w = 3\%$ was used. The applied pressure was $P_o = 0.044$ MPa (=6.3 psi). The simulations were run using mean particle radii of $\mu_p = 10$ nm and $\mu_p = 100$ nm, and both CA and HHF-CC assumptions were employed.

Figure 11 shows a reasonable agreement between the results of the experiments and the model. The maximum MRR occurs at around pH 8, as determined by experiments and the model for the alumina slurry (Fig. 11a). However, for the silica slurry (Fig. 11b), the model predicts the maximum MRR to occur near pH 5, while it was found near pH 4 in the experiments. The effect of the double-layer forces f_{dl} was small when the mean particle radius $\mu_p = 100$ nm was used in the simulations, whereas a significant influence of double-layer forces was observed when $\mu_p = 10$ nm was used. The simulations underpredict the overall effect of pH for both

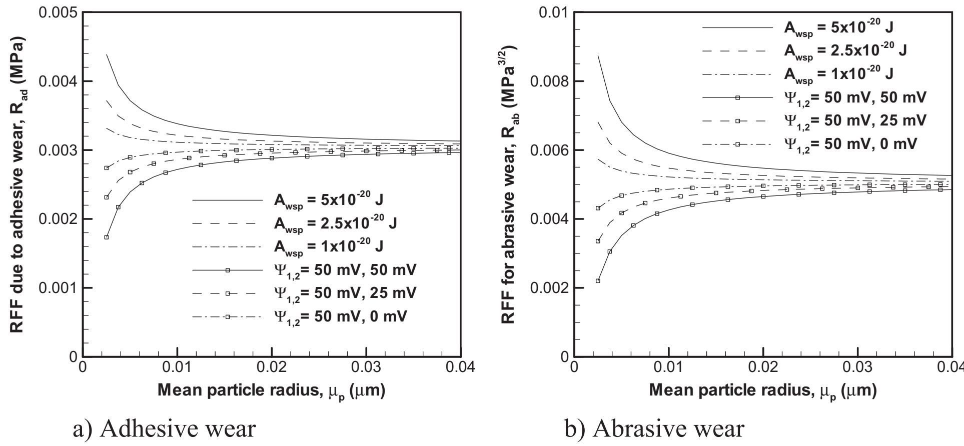

Figure 10. The effect of mean particle radius μ_p on RFF for (a) adhesive R_{ad} and (b) abrasive wear R_{ab} in the presence of surface forces.

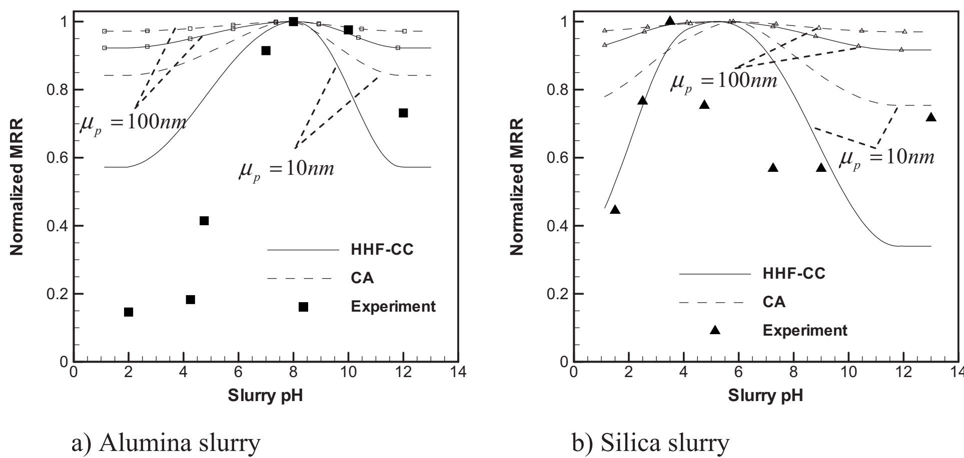

Figure 11. The variation of normalized MRR with slurry pH using (a) alumina and (b) silica slurry.[19]

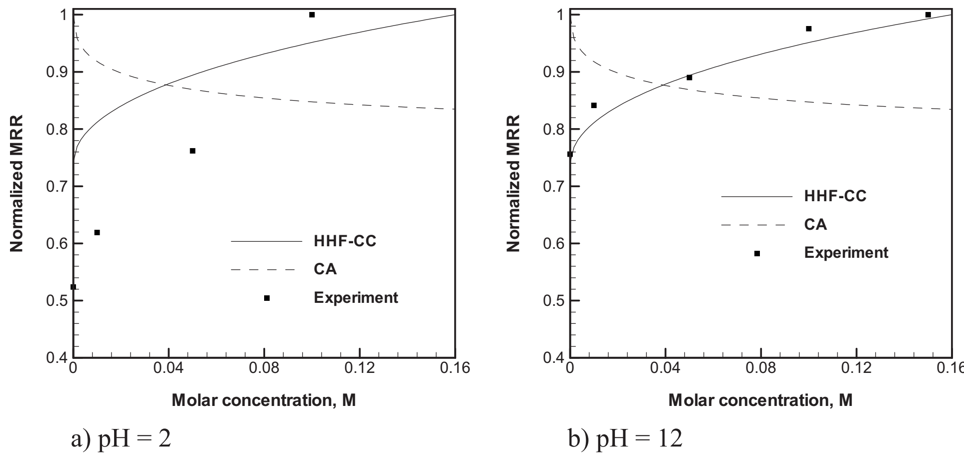

Figure 12. The variation of normalized MRR of tantalum film polished with alumina slurry as a function of molar concentration M at (a) pH 2 and (b) pH 12.[19]

Downloaded 12 Jan 2010 to 129.10.64.116. Redistribution subject to ECS license or copyright; see http://www.ecsdl.org/terms_use.jsp

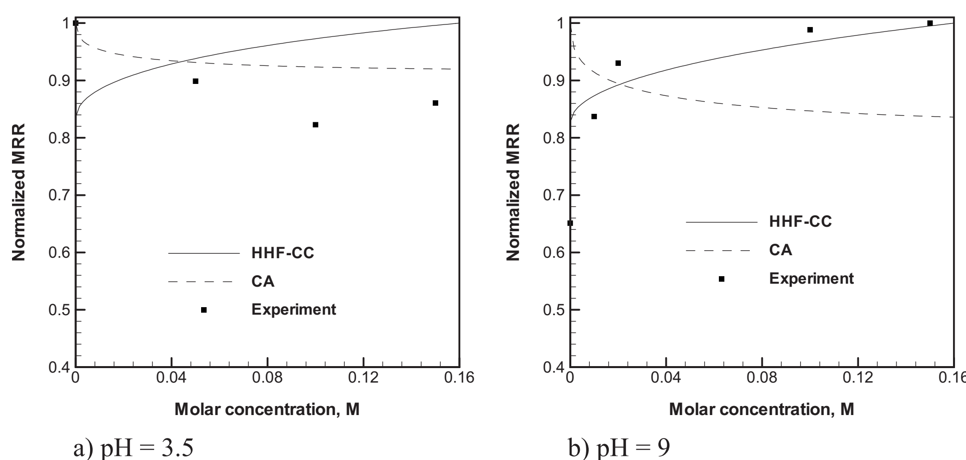

Figure 13. The variation of normalized MRR of tantalum film polished with silica slurry as a function of molar concentration M at (a) pH 3.5 and (b) pH 9.[19]

the alumina and silica slurry. The HHF-CC assumption yields better quantitative agreement with the experiment results than the CA assumption.

The experiments reported by Ramarajan et al.[19] also included the effect of the molar concentration of KCl ions in the slurry. The ionic molar concentration controls the magnitude of the double-layer force and seems to have a strong effect on the MRR, as shown in Fig. 12 and 13. The molar ion concentration M is used in the model for calculating the double-layer forces f_{dl} with CA and HHF-CC assumptions. The particle radius of $\mu_p = 10$ nm was used in the simulations, along with the other parameters, as given before. The opposite trends for the variation in the MRR with molar concentration were predicted for the CA and HHF-CC assumptions. Comparing the experiment and the model results plotted in Fig. 12 and 13, the double-layer force calculated based on the HHF-CC assumption results in a better agreement with the experiments for the alumina (pH 2 and 12) and silica (pH 9) slurries. These results indicate lower MRR with lower molar concentration M. An opposite trend is seen for the silica slurry when pH was adjusted to pH 3.5. In this case, the MRR decreased with a higher molar concentration, as predicted by the CA assumption.

The comparisons presented in Fig. 11-13 show that the effect of pH was, in general, underpredicted by the model. This finding could be attributed to various effects. For example, the thickness and the hardness of the passivated layer are strong functions of slurry pH.[10,41,42] The slurry pH could also influence the effective particle size, as the colloidal stability of slurry particles depends on surface forces acting between particles. Furthermore, the number of active particles could also be influenced by surface forces. Similar to the colloidal behavior of particles, due to particle–particle interactions, the wafer and the particle also interact with each other, and this interaction may have a strong effect on several active particles. A strong repulsive double-layer force f_{dl} between the wafer and the particle may cause the number of active particles n_a to decrease as well as having a negative effect on the wafer–particle contact force f_w for the active particles.

Conclusions

In this work, the effects of surface forces between abrasive particles and a wafer were incorporated into a contact mechanics based on a hierarchical material removal model. It was shown that the van der Waals force causes the MRR to increase. The double-layer forces, which are mostly negative, cause the MRR to decrease. The magnitude of double-layer forces depends on the molar concentration of ions M and the zeta potential of the wafer and the particles $\Psi_{1,2}$. Therefore, as the zeta potential $\Psi_{1,2}$ varies with slurry pH, the model results for the MRR become a function of slurry pH.

The work shows that the surface force f_s is proportional to the abrasive particle radius $f_s \propto \mu_p$, where as the pad–particle contact force f_p to the square of the particle radius $f_p \propto \mu_p^2$. Thus, the surface force becomes progressively more dominant for smaller particles. If the attractive van der Waals forces are the dominant surface force component, then the RFF increases with a smaller particle size, while the opposite is true in the case where the repulsive double-layer forces are dominant. In fact, the experimental work has shown both increasing[43,44] and decreasing[45] MRRs with respect to the particle size that was found in experiments supporting this finding.

This work also showed that the relative effect of surface forces on the MRR increases for softer pads, i.e., lower E_s values and smaller particles μ_p. This can be explained by considering that stiffer pads, i.e., higher E_s values, cause the number of active particles to become smaller,[27] thus resulting in a higher mean particle contact force. As the magnitude of surface forces do not depend on E_s, the relative magnitude of the surface forces decreases stiffer pads E_s.

The experimental observations for the effect of double-layer forces were predicted well by the model when double-layer forces were calculated using the CC assumption (HHF-CC). Therefore, the HHF-CC approximation seems to be more appropriate compared to CA for estimating the magnitude of double-layer forces.

Acknowledgment

The authors thank H.C. Starck Inc. for the partial support of D.B.'s Ph.D. studies.

Northeastern University assisted in meeting the publication costs of this article.

References

1. *Chemical Mechanical Planarization of Semiconductor Materials*, M. R. Oliver, Editor, Springer, New York (2004).
2. K. W. Chen and Y. L. Wang, *J. Electrochem. Soc.*, **154**, H41 (2007).
3. W. Choi, U. Mahajan, S. M. Lee, J. Abiade, and R. K. Singh, *J. Electrochem. Soc.*, **151**, G185 (2004).
4. R. Ihnfeldt and J. B. Talbot, *J. Electrochem. Soc.*, **155**, H412 (2008).
5. S. Deshpande, S. C. Kuiry, M. Klimov, Y. Obeng, and S. Seal, *J. Electrochem. Soc.*, **151**, G788 (2004).
6. J. Hernandez, P. Wrschka, and G. S. Oehrlein, *J. Electrochem. Soc.*, **148**, G389 (2001).
7. V. H. Nguyen, R. Daamen, H. van Kranenburg, P. van der Velden, and P. H. Woerlee, *J. Electrochem. Soc.*, **150**, G689 (2003).
8. G. Xu, H. Liang, J. Zhao, and Y. Li, *J. Electrochem. Soc.*, **151**, G688 (2004).
9. S. Y. Chiu, Y. L. Wang, C. P. Liu, S. C. Chang, G. J. Hwang, M. S. Feng, and C. F. Chen, *Thin Solid Films*, **498**, 60 (2006).
10. S. C. Kuiry, S. Seal, W. Fei, J. Ramsdell, V. H. Desai, Y. Li, S. V. Babu, and B. Wood, *J. Electrochem. Soc.*, **150**, C36 (2003).
11. G. Lim, J. H. Lee, J. Kim, H. W. Lee, and S. H. Hyun,*Wear*, **257**, 863 (2004).
12. Y. J. Seo and W. S. Lee, *Mater. Sci. Eng., B*, **118**, 281 (2005).
13. B. C. Lee, D. J. Duquette, and R. J. Gutmann, *Mater. Res. Soc. Symp. Proc.*, **671**, 2.7.1, (2001).
14. Q. Luo, D. R. Campbell, and S. V. Babu, *Langmuir*, **12**, 3563 (1996).
15. Y. K. Hong, J. H. Han, T. G. Kim, J. G. Park, and A. A. Busnaina, *J. Electrochem.*

Downloaded 12 Jan 2010 to 129.10.64.116. Redistribution subject to ECS license or copyright; see http://www.ecsdl.org/terms_use.jsp

Soc., **154**, H36 (2007).
16. Y. J. Kang, Y. K. Hong, J. H. Song, I. K. Kim, and J. G. Park, *Mater. Res. Soc. Symp. Proc.*, **867**, 7.5.1 (2005).
17. T. Gopal and J. B. Talbot, *J. Electrochem. Soc.*, **153**, G622 (2006).
18. W. Choi, J. Abiade, S. Lee, and R. K. Singh, *J. Electrochem. Soc.*, **151**, G512 (2004).
19. S. Ramarajan, Y. Li, M. Hariharaputhiran, Y. S. Her, and S. V. Babu, *Electrochem. Solid-State Lett.*, **3**(5), 232 (2000).
20. S. Hegde and S. V. Babu, *Electrochem. Solid-State Lett.*, **7**, G316 (2004).
21. W. C. Chen, S. C. Lin, B. T. Dai, and M. S. Tsai, *J. Electrochem. Soc.*, **146**, 3004 (1999).
22. R. Biswas, Y. Han, P. Karra, P. Sherman, and A. Chandra, *J. Electrochem. Soc.*, **155**, D534 (2008).
23. A. Chandra, P. Karra, A. F. Bastawros, R. Biswas, P. J. Sherman, S. Armini, and D. A. Lucca, *CIRP Ann.*, **57**, 559 (2008).
24. A. R. Mazaheri and G. Ahmadi, *J. Electrochem. Soc.*, **149**, G370 (2002).
25. A. R. Mazaheri and G. Ahmadi, *J. Electrochem. Soc.*, **150**, G233 (2003).
26. F. Zhang, A. A. Busnaina, and G. Ahmadi, *J. Electrochem. Soc.*, **146**, 2665 (1999).
27. D. Bozkaya and S. Muftu, *J. Electrochem. Soc.*, **156**, H890 (2009).
28. D. Bozkaya and S. Müftü, *ASME J. Tribol.*, **130**, 041401 (2008).
29. J. Tichy, J. A. Levert, L. Shan, and S. Danyluk, *J. Electrochem. Soc.*, **146**, 1523 (1999).
30. L. J. Borucki, T. Sun, Y. Zhuang, D. Slutz, and A. Philipossian, in *Proceedings of the MRS Spring Conference 2009*, PV 1157-E01-02, Materials Research Society (2009).
31. D. Maugis, *Contact, Adhesion and Rupture of Elastic Solids*, Springer-Verlag, Berlin, Germany (2000).
32. J. N. Israelachvili, *Intermolecular and Surface Forces*, Academic, New York (1992).
33. P. C. Hiemenz, *Principles of Colloid and Surface Chemistry*, Marcel Dekker, New York (1986).
34. G. R. Wiese and T. W. Healy, *Trans. Faraday Soc.*, **66**, 490 (1970).
35. S. J. Usui, *J. Colloid Interface Sci.*, **44**, 107 (1973).
36. J. Gregory, *J. Colloid Interface Sci.*, **51**, 44 (1975).
37. H. Shan, Ph.D. Thesis, Northeastern University, Boston, MA (2006).
38. E. Rabinowicz, *Friction and Wear of Materials*, John Wiley & Sons, New York (1995).
39. K. L. Johnson, *Contact Mechanics*, Cambridge University Press, Cambridge, U.K. (1985).
40. K. Cooper, A. Gupta, and S. Beaudoin, *J. Electrochem. Soc.*, **148**, G662 (2001).
41. S. B. Akonko, S. Y. Li, M. Ziomek-Moroz, J. Hawk, A. Miller, and K. Cadien, *Wear*, **259**, 1299 (2005).
42. A. Jindal and S. V. Babu, *J. Electrochem. Soc.*, **151**, G709 (2004).
43. D. Tamboli, G. Banerjee, and M. Waddell, *Electrochem. Solid-State Lett.*, **7**, F62 (2004).
44. J. Y. Lai, Ph.D. Thesis, Massachusetts Institute of Technology, Cambridge, MA (2001).
45. M. Bielmann, U. Mahajan, and R. K. Singh, *Electrochem. Solid-State Lett.*, **2**, 401 (1999).

Downloaded 12 Jan 2010 to 129.10.64.116. Redistribution subject to ECS license or copyright; see http://www.ecsdl.org/terms_use.jsp